How to cite: *Angew. Chem. Int. Ed.* **2022,** *61,* e202202727
International Edition: doi.org/10.1002/anie.202202727
German Edition: doi.org/10.1002/ange.202202727

Computational Catalysis **Hot Paper**

Mapping Active Site Geometry to Activity in Immobilized Frustrated Lewis Pair Catalysts

*Shubhajit Das, Ruben Laplaza, J. Terence Blaskovits, and Clémence Corminboeuf**

Abstract: The immobilization of molecular catalysts imposes spatial constraints on their active site. We reveal that in bifunctional catalysis such constraints can also be utilized as an appealing handle to boost intrinsic activity through judicious control of the active site geometry. To demonstrate this, we develop a pragmatic approach, based on nonlinear scaling relationships, to map the spatial arrangements of the acid–base components of frustrated Lewis pairs (FLPs) to their performance in the catalytic hydrogenation of CO_2. The resulting activity map shows that fixing the donor–acceptor centers at specific distances and locking them into appropriate orientations leads to an unforeseen many-fold increase in the catalytic activity of FLPs compared to their unconstrained counterparts.

Immobilized molecular catalysts are of great interest due to their improved stability and recyclability compared to fully homogeneous catalysts.[1–4] A direct consequence of this immobilization is that the active site of the catalyst becomes geometrically constrained, adopting a rigidified conformation that is less susceptible to change over the course of the reaction. Constrained reaction centers are key to the activity of a large diversity of catalytic systems, ranging from enzyme pockets to the ordered molecular frameworks of porous materials.[5–7] While activity in such catalysts is primarily determined by the molecular composition of the active site (hereby denoted as *intrinsic* activity), the constrained environment may have a substantial and unforeseen impact on its performance.[8–10] This is especially true for a bifunctional catalyst that relies on cooperativity between two spatially proximal components with complementary chemical features.[11–13] Understanding and predicting the degree to which spatial constraints affect the intrinsic behaviour of the immobilized catalysts is therefore an indispensable endeavour. Although the chemical composition of homogeneous and heterogeneous catalysts has often been directly tied to their performance, a holistic understanding of the consequences of catalyst immobilization on activity and, by extension, the (quantitative) relationship between active site geometry and activity, are currently missing. This crucial connection is required to formulate design principles for the construction of such hybrid active sites.

Here, we aim to bridge this knowledge gap by analyzing how immobilization controls the intrinsic activity of frustrated Lewis pairs (FLPs),[14–19] reactive combinations of Lewis acids (LAs) and bases (LBs), to catalyze the hydrogenation of CO_2 to formate.[20–23] Several groups have incorporated Lewis pair units in the solid supports of metal/covalent organic frameworks,[24–31] zeolites,[32] mesoporous silica,[33] metal oxide surfaces,[34–36] and within heterogeneous intramolecular scaffolds[37] to achieve various catalytic transformations.[38] Given that the reactivity of this catalyst family is derived from the physical proximity of the LA and LB components,[39,40] it is expected that their relative positioning in these rigid active sites affects performance: components placed too far apart will show little cooperativity, while sites too close together will create sterically congested reaction environments. In this work, we develop a general approach based on nonlinear scaling relationships to capture the intimate connection between the geometric arrangement of the donor–acceptor sites and their performance. Our results reveal that geometric constraints can be utilized to enhance the intrinsic activity of bifunctional catalysts by judicious spatial control of the components.

Figure 1a illustrates the generalized catalytic cycle for direct FLP-catalyzed CO_2 hydrogenation to formate on the basis of our computations and previous experimental and computational studies.[41–46] The mechanism involves the heterolytic cleavage of H_2 by the LA-LB pair **1**, leading to the formation of the ion-pair **2** through **TS1**. Binding of CO_2 results in intermediate **3**, which upon hydride transfer (HT) via **TS2** leads to the formation of **4**, featuring the formate bound to the LA and LB units. The catalytic cycle is closed upon extraction of the formate by a sacrificial reagent (e.g. additional base or boron species) and regeneration of the catalyst.

To characterize the evolution of the active site geometry during the hydrogenation cycle, we invoke two structural descriptors: the distance between the central donor and

[*] Dr. S. Das, Dr. R. Laplaza, J. T. Blaskovits, Prof. Dr. C. Corminboeuf
Laboratory for Computational Molecular Design, Institute of Chemical Sciences and Engineering, Ecole Polytechnique Federale de Lausanne
1015 Lausanne (Switzerland)
E-mail: clemence.corminboeuf@epfl.ch
Dr. R. Laplaza, Prof. Dr. C. Corminboeuf
National Center for Competence in Research-Catalysis (NCCR-Catalysis), Ecole Polytechnique Federale de Lausanne
1015 Lausanne (Switzerland)

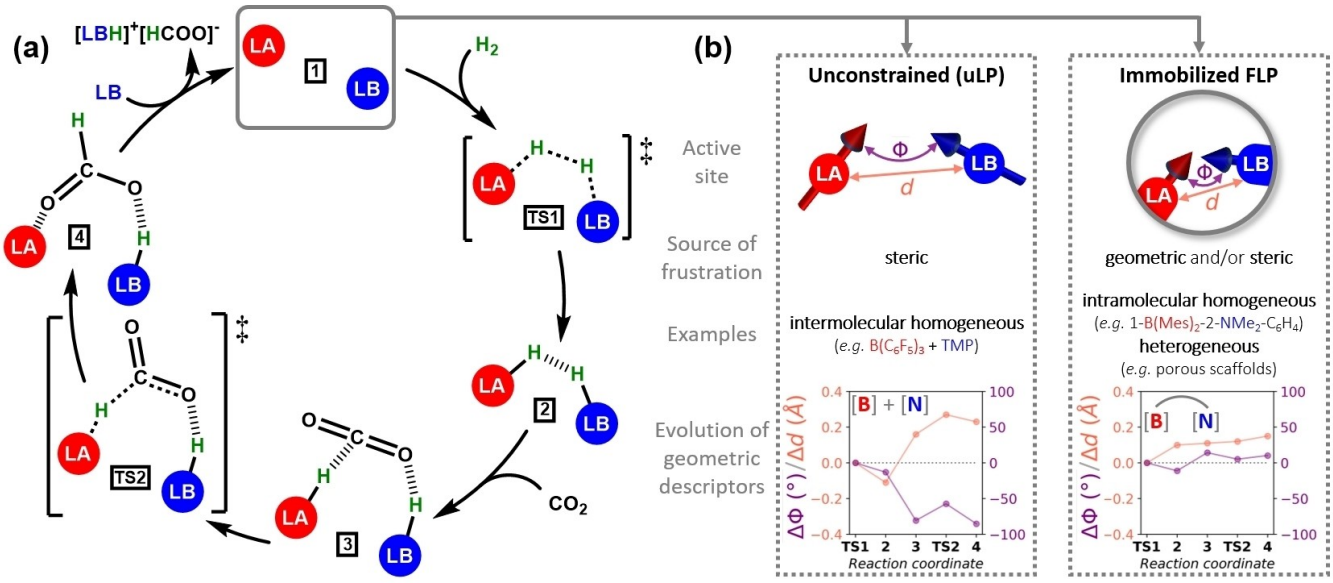

Figure 1. a) Catalytic cycle for the FLP-catalyzed direct hydrogenation of CO_2 to formate. LA = Lewis acid; LB = Lewis base. Dotted lines represent the bonds formed and cleaved in the transition states, and dashed lines represent other non-covalent interactions. Off-cycle resting states such as an FLP-CO_2 adduct or a quenched LA–LB dative adduct are omitted for the sake of generality. The cycle shown here uses an additional LB molecule as the sacrificial agent, providing the driving force for product extraction. b) Schematic depiction of active site constructions, sources of frustration, literature examples and evolution of the active site geometry during the course of hydrogenation in unconstrained (uLP, left) and immobilized (right) catalysts. The geometry of the active site is characterized by two descriptors, the distance d (orange) and angle Φ (purple) between LA and LB. Geometry-based results are shown for representative unconstrained and intramolecular (constrained) boron-nitrogen FLPs (BF_3/pyridine and 2-$BMe_2C_5H_4N$, respectively), where Δd and $\Delta\Phi$ denote the variation in the descriptors with respect to the **TS1** structure. TMP = 2,2,6,6-tetramethylpiperidine; Mes = 2,4,6-$Me_3C_6H_2$.

acceptor atoms (d) and their orientation relative to one another (Φ, see Figure 1b and Figure S1 for a more detailed description). These are easily extracted through analysis of the molecular geometries and are, crucially, transferable among all the steps of the cycle. Monitoring these descriptors for an unconstrained intermolecular B/N Lewis pair (denoted hereafter as *uLP*, Scheme 1), BF_3 and pyridine,[47] reveals that the structural signatures during the initial (H_2 cleavage) and subsequent (HT/formate release) stages of the cycle are markedly different (see Figure 1b, bottom left and Figures S2, S3 for structures and corresponding d/Φ values). While hydrogen cleavage (**TS1**) occurs in nearly perpendicular Lewis centres with a sufficiently small separation to establish a cooperative interaction with the incoming molecule, HT (**TS2**) takes place with a larger B–N separation and an acute orientation to allow for the necessary contact between the hydride/proton pair with the carbonyl bond. If the active sites are constrained (i.e., fixed d and Φ), the structural adaption of the LA–LB subunits to a given reaction step is restricted, resulting in distinct binding orientations compared to the uLP. The loss of flexibility of the reactive centers in an immobilized catalyst leads to preferential (de)stabilization of the reactive intermediates and transition states, altering the energy profile and catalytic activity compared to the corresponding fully flexible counterpart. Thus, each constrained geometry may be associated with a different catalytic activity.

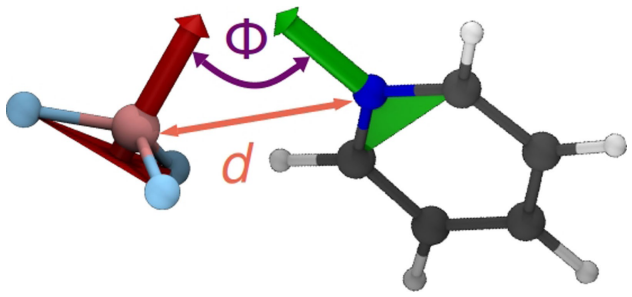

Scheme 1. Schematic depiction of the two geometric descriptors used to monitor the active site of the BF_3-pyridine FLP. d is trivially calculated as the distance between the central B and N atoms of the LA and LB units, respectively. Φ is defined as the angle between the open coordination sites of the Lewis components.

Figure 2a illustrates the relative stability (ΔG_{RRS}) for each intermediate and transition state in the hydrogenation cycle upon elongation of the LA–LB distance, while letting the orientation adapt freely, as evaluated by density functional theory (see Supporting Information for computational details). The resulting Morse curve relationships observed for each catalytic cycle species are intuitive: at very short B–N distances, the reaction cavity is not spacious enough to accommodate the substrate molecules, leading to steric repulsion, while at longer distances cooperative reactivity between the donor and acceptor sites is gradually lost. Both situations lead to less stable reaction intermediates and higher-lying transition states, between which an LA–LB distance exists for the optimal stabilization of each sta-

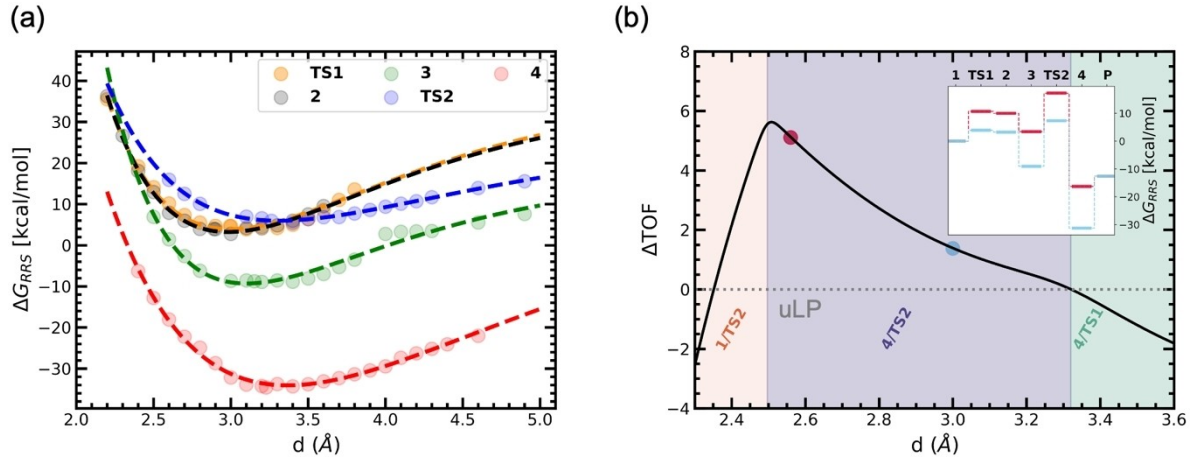

Figure 2. a) Energy-distance scaling relationship showing the variation of free energies with LA–LB separation for each intermediate and transition state in the CO_2 hydrogenation cycle catalyzed by BF_3/Py Lewis pair, fitted with Morse potentials. Free energies are given **r**elative to the **r**esting **s**tate ($\Delta\mathbf{G}_{RRS}$), where the resting state is taken to be the separated reactants **1**. Equation details and mean absolute errors are given in Section S2 and Figure S4, respectively. b) Variation of the computed TOF for CO_2 hydrogenation to formate as a function of LA–LB separation. The volcano-shaped curve is built from the energy-distance scaling relationships obtained for each reaction intermediate and transition state involved in the catalytic cycle featuring the BF_3/pyridine Lewis pair. ΔTOF = log (TOF/TOF$_{uLP}$). Inset shows hydrogenation profiles for two representative points from the TOF curve. **P** denotes the hydrogenation product.

tionary point. This corresponds to the LA–LB distance in the minimum energy geometry of the uLP. To capture these variations for each intermediate and transition state, we fit the ΔG_{RRS} values to a Morse potential (as shown by the dotted lines in Figure 2a). These fitted curves correspond to scaling relationships (SRs) that allow for the prediction of the hydrogenation profile from the LA–LB separation alone. Such geometry-based relationships are analogous to the energy-based linear SRs often utilized in homogeneous and heterogeneous catalysis, in which the relative energy of one (or several) reaction intermediate(s) is used as the descriptor to predict catalytic cycle energetics and, in turn, catalyst efficiency.[48–54]

The Morse potential-based SRs shown in Figure 2a can be employed to retrieve the computed turnover frequency (TOF) as a function of the active site geometry (fixed d). The plausible gain or loss in performance due to active site immoblization is thereby assessed by estimating the resulting relative TOF (ΔTOF) with respect to the value derived from the hydrogenation profile of the uLP (see Supporting Information for details). The TOF resulting from the post-processing of these nonlinear SRs takes the shape of a volcano-type curve, as shown in Figure 2b. Here, a particular distance can be identified at which the intermediate and transition state energies lie in such a way that they provide the smallest overall energy penalty over the course of the reaction (the peak shown near 2.5 Å). When compared to the activity of the uLP (the TOF represented by the grey horizontal line in Figure 2b), it is clear that the energy profile of a Lewis pair constrained at a distance corresponding to the volcano peak is significantly more favorable, leading to a TOF up to five orders of magnitude higher. This increase is rationalized by the rapid destabilization of intermediate **4** (due to progressively more constrained geometries) compared to the other intermediates and transition states in the profile as the B–N separations are gradually lowered (see Figure 2b inset). In fact, the dominance of intermediate **4** in controlling the overall activity is apparent when the TOF curve is divided into regions corresponding to the reaction step(s) that are the most energetically demanding in the hydrogenation cycle.[55]

To include the influence of the LA–LB orientation in the above picture, $\Delta\mathbf{G}_{RRS}$ values are fitted to a modified Morse potential, which is a function of both variables, d and Φ (see Supporting Information for details). The resulting SRs (see Figures S6–S10) are then leveraged to construct a complete picture of the relationship between the geometry of a given FLP environment and the resulting TOF in the form of an activity map (see Figure 2a). Here, the color corresponds to the gain (positive values) or loss (negative values) in performance relative to the uLP. Maximum efficiency for the immobilized Lewis pair environment is therefore obtained when the LA-LB units are fixed at a distance of 2.5–2.8 Å (vertical dashed lines) and oriented at an angle between 90°–135° (horizontal dashed lines). The associated peak performance is estimated to be approximately eleven orders of magnitude higher than the uLP. The shape of the TOF peak indicates that the angle is a more strict requirement than the distance: high efficiency can be obtained over a relatively large range of distances provided that the LA–LB orientation is appropriate, while at a fixed distance, the TOF drops steeply outside the ideal Φ range. The effect of "off-cycle" intermediates, such as a CO_2 adduct of uLP, on the calculated TOF is shown in Figure S16.

Inspection of Figure 3b reveals that the diminished performance observed at lower Φ values (<50°, blue region) is a consequence of the LA–LB units not being oriented properly for the H_2 activation step. This results in a high-lying **TS1**, coupled to energetically unfavourable product

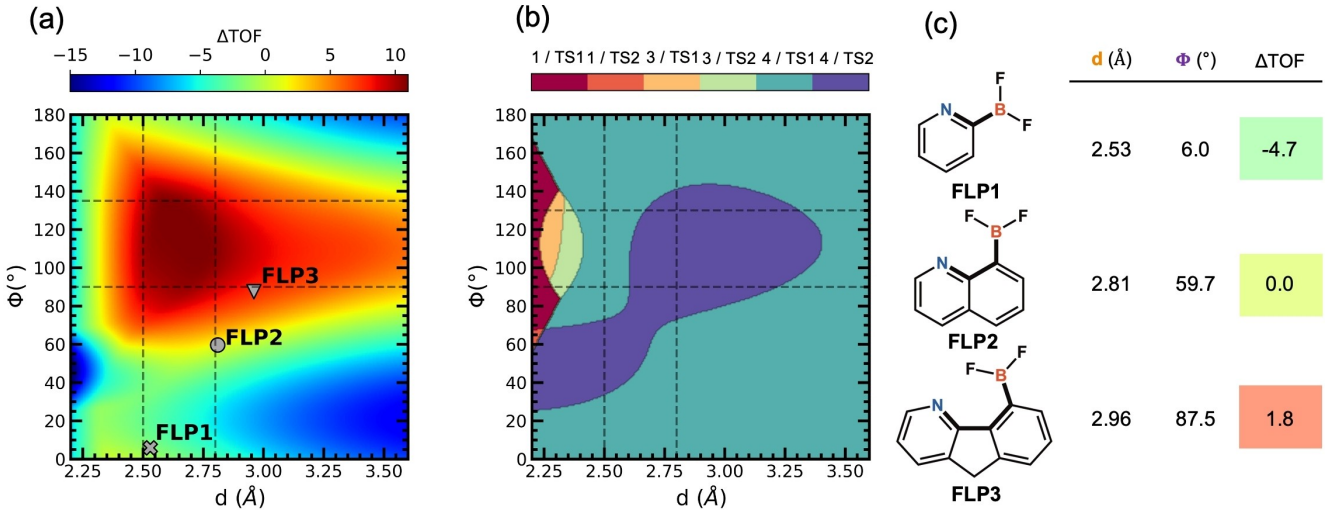

Figure 3. a) Activity map describing the TOF for uLP-catalyzed CO_2 hydrogenation as a function of LA-LB separation, *d*, and their relative orientation, *Φ*, plotted along the *x* and *y* axes, respectively, constructed from the 2D distance-angle-energy scaling relationships obtained for each reaction intermediate and transition state (b) Map in which each grid point is colored according to the identity of the intermediate and transition state that determines the highest barrier in the corresponding free energy profile. The vertical and horizontal dashed lines indicate the range of *d* and *Φ*, respectively, corresponding to the maximum activity region. c) Chemical composition of the intramolecular FLPs that are mapped in Figure 3a and the geometric descriptor values extracted from the corresponding intermediate **2**, along with the TOF values estimated from their fully computed profiles. All TOF values are given in the logarithmic scale.

release. In fact, for most of the range of possible geometric arrangements, the activity is essentially determined by **4** and **TS1**. The greatest variation is found in the hotspot ($\Phi = 90°$–$135°$) in the plot; while at lower (2.4–2.6 Å) and higher (3.4–3.6 Å) distances **TS1** dominates the activity along with **4**, **TS2** dominates at intermediate *d* values. This *Φ* range corresponds to the favorable LA–LB orientation for H_2 activation, implying that preferential promotion of this step through immobilization could be a general strategy to enhance catalyst efficiency.

To confirm that the activity map correctly captures the impact of geometric constraints on the catalytic performance, we mapped realistic[56–58] intramolecular FLPs, featuring similar chemical compositions[59] but different active site geometries, onto Figure 3a. Figure 3c depicts the corresponding structures in which the $–BF_2$ LA unit is embedded into three different aromatic nitrogen-containing scaffolds. The B and N centres in FLP1, FLP2 and FLP3 are separated by 1, 2 and 3 carbon atoms, respectively, covering a range of B–N distances and orientations. With the activity map, it is possible to predict the relative TOFs based solely on geometric descriptors (*d* and *Φ*) without resorting to the computation of their full kinetic profiles. Given that the flexibility of the LA-LB units in these realistic scaffolds is significantly restricted during the course of the hydrogenation process, albeit not fully immobilized, it is necessary to choose a particular reaction step from which geometric parameters are extracted. We selected the *d* and *Φ* describing intermediate **2**, as this structure captures the geometric response of the FLP environment to the inclusion of the H_2 molecule. The relative ordering of activity predicted by the map is FLP3>FLP2>FLP1, where FLP3 is located in a higher activity region of Figure 3a. This prediction is validated by computing the full CO_2 hydrogenation profiles of FLP1, FLP2 and FLP3 (see Figure S11), which yield relative TOFs of −4.7, 0.0 and 1.8 (compared to the uLP reference), respectively, in agreement with the relative values predicted from the map. Overall, these results demonstrate that geometry-based activity maps built upon well-suited functions can be applied to rapidly screen immobilized FLPs to identify catalyst architectures with active site geometries which promote a highly efficient catalytic process.

The predictive power of the tool is further demonstrated by examining the previously reported experimental results by Fontaine et al. on the reactivity of intramolecular amine-borane FLPs towards CO_2 hydrogenation. While hydrogenation products were observed for 1-NMe_2-2-$BR2_2$-C_6H_4 (where R = mesityl or 2,4,5-$Me_3C_6H_2$) in the presence of CO_2 and H_2,[42] an analogous FLP on a similar benzene scaffold, 1-TMP-2-BBN-C_6H_4 (TMP = 2,2,6,6-tetramethylpiperidine, BBN = 9-borabicyclo[3.3.1]nonane), failed to exhibit any reactivity in similar conditions.[60] Using the geometric parameters extracted from the corresponding intermediate **2**, our model predicts a 10^7-fold difference in reactivity between the active form (1-NMe_2–2-BH_2–C_6H_4)of the former ($d = 2.79$ Å and $\Phi = 114°$, within the hotspot shown in Figure 3a) and the latter FLPs ($d = 2.92$ Å and $\Phi = 76°$, in a significantly lower activity region). Therefore, the geometry-activity model predicts negligible activity of 1-TMP-2-BBN-C_6H_4 with respect to 1-NMe_2–2-BR_2–C_6H_4, due to the geometric constraints imposed by the bulkier BBN and TMP substituents on the acid and base centers, in agreement with the experimentally observed trend. While we remain cautious in attributing this divergence in reactivity exclusively to differences in the geometry of the

active site, we note that the chemical environments of the acid and base sites are sufficiently similar to enable a qualitative comparison of these FLPs (see section S3 for details).

In conclusion, we highlight the potential of constraining the Lewis acid and base components of FLP catalysts as a means to boost their intrinsic activity for the direct hydrogenation of CO_2 to formate. We demonstrate this by mapping the bifunctional active site geometry to its performance based on nonlinear scaling relationships that establish a connection between the catalytic cycle energetics and the separation distance and relative orientation of the donor–acceptor units. The resulting map serves as a guide to recognize the specific geometric arrangements of the Lewis components which lead to significantly enhanced activity. We envision that the approach developed here can be exploited for accelerating discovery of optimally immobilized bifunctional molecular environments to drive efficient catalytic transformations.

Acknowledgements

This project was funded by GAZNAT. The authors thank EPFL for computational resources. This publication was created as part of NCCR Catalysis (grant number 180544 funding R. L.), a National Centre of Competence in Research funded by the Swiss National Science Foundation. Sergi Vela, Matthew D. Wodrich and Simone Gallarati are thanked for useful discussions. Raimon Fabregat is thanked for the TOC graphic. Open access funding provided by Ecole Polytechnique Federale de Lausanne.

Conflict of Interest

The authors declare no conflict of interest.

Data Availability Statement

All data and python scripts to fit the modified Morse potentials and generate the figures in this communication are available at https://doi.org/10.5281/zenodo.6451293

Keywords: CO_2 Hydrogenation · Frustrated Lewis Pairs · Geometry–Activity Relationships · Immobilized Catalysts · Scaling Relationships

[1] M. Benaglia, A. Puglisi, *Catalyst Immobilization: Methods and Applications*, Wiley, Hoboken, **2019**.
[2] J. A. Gladysz, *Chem. Rev.* **2002**, *102*, 3215.
[3] R. Ye, J. Zhao, B. B. Wickemeyer, F. D. Toste, G. A. Somorjai, *Nat. Catal.* **2018**, *1*, 318.
[4] D. De Vos, I. F. Vankelecom, P. A. Jacobs, *Chiral Catalyst Immobilization and Recycling*, Wiley, Hoboken, **2008**.
[5] B. Mitschke, M. Turberg, B. List, *Chem* **2020**, *6*, 2515.
[6] A. Küchler, M. Yoshimoto, S. Luginbühl, F. Mavelli, P. Walde, *Nat. Nanotechnol.* **2016**, *11*, 409.
[7] A. Bhan, E. Iglesia, *Acc. Chem. Res.* **2008**, *41*, 559.
[8] Z. An, Y. Guo, L. Zhao, Z. Li, J. He, *ACS Catal.* **2014**, *4*, 2566.
[9] R. Alamillo, A. J. Crisci, J. M. R. Gallo, S. L. Scott, J. A. Dumesic, *Angew. Chem. Int. Ed.* **2013**, *52*, 10349; *Angew. Chem.* **2013**, *125*, 10539.
[10] J. Long, G. Liu, T. Cheng, H. Yao, Q. Qian, J. Zhuang, F. Gao, H. Li, *J. Catal.* **2013**, *298*, 41.
[11] A. M. Robinson, J. E. Hensley, J. W. Medlin, *ACS Catal.* **2016**, *6*, 5026.
[12] D. H. Paull, C. J. Abraham, M. T. Scerba, E. Alden-Danforth, T. Lectka, *Acc. Chem. Res.* **2008**, *41*, 655.
[13] K. Motokura, T. Baba, Y. Iwasawa, *Bridging Heterogeneous and Homogeneous Catalysis*, Wiley-VCH, Weinheim, **2014**, pp. 1–20.
[14] G. Erker, D. W. Stephan, *Frustrated Lewis Pairs*, Springer, Heidelberg, **2013**.
[15] D. W. Stephan, G. Erker, *Angew. Chem. Int. Ed.* **2010**, *49*, 46; *Angew. Chem.* **2010**, *122*, 50.
[16] D. W. Stephan, G. Erker, *Angew. Chem. Int. Ed.* **2015**, *54*, 6400; *Angew. Chem.* **2015**, *127*, 6498.
[17] G. Erker, D. W. Stephan, *Frustrated Lewis Pairs II*, Springer Berlin Heidelberg, Berlin, **2013**.
[18] D. W. Stephan, *J. Am. Chem. Soc.* **2015**, *137*, 10018.
[19] D. W. Stephan, *Science* **2016**, *354*, eaaf7229.
[20] W.-H. Wang, Y. Himeda, J. T. Muckerman, G. F. Manbeck, E. Fujita, *Chem. Rev.* **2015**, *115*, 12936.
[21] A. Álvarez, A. Bansode, A. Urakawa, A. V. Bavykina, T. A. Wezendonk, M. Makkee, J. Gascon, F. Kapteijn, *Chem. Rev.* **2017**, *117*, 9804.
[22] J. Klankermayer, S. Wesselbaum, K. Beydoun, W. Leitner, *Angew. Chem. Int. Ed.* **2016**, *55*, 7296; *Angew. Chem.* **2016**, *128*, 7416.
[23] Q. Liu, L. Wu, R. Jackstell, M. Beller, *Nat. Commun.* **2015**, *6*, 5933.
[24] Z. Niu, W. D. C. Bhagya Gunatilleke, Q. Sun, P. C. Lan, J. Perman, J.-G. Ma, Y. Cheng, B. Aguila, S. Ma, *Chem* **2018**, *4*, 2587.
[25] S. Shyshkanov, T. N. Nguyen, A. Chidambaram, K. C. Stylianou, P. J. Dyson, *Chem. Commun.* **2019**, *55*, 10964.
[26] S. Shyshkanov, T. N. Nguyen, F. M. Ebrahim, K. C. Stylianou, P. J. Dyson, *Angew. Chem. Int. Ed.* **2019**, *58*, 5371; *Angew. Chem.* **2019**, *131*, 5425.
[27] Q. Meng, Y. Huang, D. Deng, Y. Yang, H. Sha, X. Zou, R. Faller, Y. Yuan, G. Zhu, *Adv. Sci.* **2020**, *7*, 2000067.
[28] Y. Zhang, P. C. Lan, K. Martin, S. Ma, *Chem Catalysis* **2022**, *2*, 439–457.
[29] Q. Liu, Q. Liao, J. Hu, K. Xi, Y.-T. Wu, X. Hu, *J. Mater. Chem. A* **2022**, *10*, 7333–7340.
[30] J. Ye, J. K. Johnson, *ACS Catal.* **2015**, *5*, 6219.
[31] J. Ye, J. K. Johnson, *ACS Catal.* **2015**, *5*, 2921.
[32] H. Lee, Y. N. Choi, D.-W. Lim, M. M. Rahman, Y.-I. Kim, I. H. Cho, H. W. Kang, J.-H. Seo, C. Jeon, K. B. Yoon, *Angew. Chem. Int. Ed.* **2015**, *54*, 13080; *Angew. Chem.* **2015**, *127*, 13272.
[33] M. V. Zakharova, N. Masoumifard, Y. Hu, J. Han, F. Kleitz, F.-G. Fontaine, *ACS Appl. Mater. Interfaces* **2018**, *10*, 13199.
[34] L. Wang, G. Kehr, C. G. Daniliuc, M. Brinkkötter, T. Wiegand, A.-L. Wübker, H. Eckert, L. Liu, J. G. Brandenburg, S. Grimme, G. Erker, *Chem. Sci.* **2018**, *9*, 4859.
[35] Y. Dong, K. K. Ghuman, R. Popescu, P. N. Duchesne, W. Zhou, J. Y. Loh, A. A. Jelle, J. Jia, D. Wang, X. Mu, C. Kübel, L. Wang, L. He, M. Ghoussoub, Q. Wang, T. E. Wood, L. M. Reyes, P. Zhang, N. P. Kherani, C. V. Singh, G. A. Ozin, *Adv. Sci.* **2018**, *5*, 1700732.
[36] S. Zhang, Z.-Q. Huang, Y. Ma, W. Gao, J. Li, F. Cao, L. Li, C.-R. Chang, Y. Qu, *Nat. Commun.* **2017**, *8*, 1.
[37] N. Bouchard, F.-G. Fontaine, *Dalton Trans.* **2019**, *48*, 4846.

[38] A. R. Jupp, *Frustrated Lewis Pairs*, Springer International Publishing, Cham, **2020**, pp. 237–281.
[39] T. A. Rokob, A. Hamza, A. Stirling, T. Soós, I. Pápai, *Angew. Chem. Int. Ed.* **2008**, *47*, 2435; *Angew. Chem.* **2008**, *120*, 2469.
[40] T. A. Rokob, I. Bakó, A. Stirling, A. Hamza, I. Pápai, *J. Am. Chem. Soc.* **2013**, *135*, 4425.
[41] A. E. Ashley, A. L. Thompson, D. O'Hare, *Angew. Chem. Int. Ed.* **2009**, *48*, 9839; *Angew. Chem.* **2009**, *121*, 10023.
[42] M.-A. Courtemanche, A. P. Pulis, É. Rochette, M.-A. Légaré, D. W. Stephan, F.-G. Fontaine, *Chem. Commun.* **2015**, *51*, 9797.
[43] L. Liu, N. Vankova, T. Heine, *Phys. Chem. Chem. Phys.* **2016**, *18*, 3567.
[44] S. D. Tran, T. A. Tronic, W. Kaminsky, D. Michael Heinekey, J. M. Mayer, *Inorg. Chim. Acta* **2011**, *369*, 126.
[45] T. Zhao, X. Hu, Y. Wu, Z. Zhang, *Angew. Chem. Int. Ed.* **2019**, *58*, 722; *Angew. Chem.* **2019**, *131*, 732.
[46] M. Wen, F. Huang, G. Lu, Z.-X. Wang, *Inorg. Chem.* **2013**, *52*, 12098.
[47] This selection was motivated by the fact that B/N FLPs (both intramolecular and intermoecular) were previously reported to perform hydrogenation of CO_2. Furthermore, bulky substituents, which are often used to prevent dative adduct formation in FLPs, were deliberately not included as "frustration" is artificially induced in this Lewis pair by imposing distance constraints.
[48] J. Greeley, *Annu. Rev. Chem. Biomol.* **2016**, *7*, 605.
[49] M. Busch, M. D. Wodrich, C. Corminboeuf, *Chem. Sci.* **2015**, *6*, 6754.
[50] A. J. Medford, A. Vojvodic, J. S. Hummelshøj, J. Voss, F. Abild-Pedersen, F. Studt, T. Bligaard, A. Nilsson, J. K. Nørskov, *J. Catal.* **2015**, *328*, 36.
[51] M. Anand, B. Rohr, M. J. Statt, J. K. Nørskov, *J. Phys. Chem. Lett.* **2020**, *11*, 8518.
[52] T. Bligaard, J. K. Nørskov, S. Dahl, J. Matthiesen, C. H. Christensen, J. Sehested, *J. Catal.* **2004**, *224*, 206.
[53] M. D. Wodrich, B. Sawatlon, M. Busch, C. Corminboeuf, *Acc. Chem. Res.* **2021**, *54*, 1107.
[54] M. D. Wodrich, B. Sawatlon, E. Solel, S. Kozuch, C. Corminboeuf, *ACS Catal.* **2019**, *9*, 5716.
[55] S. Kozuch, S. Shaik, *Acc. Chem. Res.* **2011**, *44*, 101.
[56] T. G. Hodgkins, D. R. Powell, *Inorg. Chem.* **1996**, *35*, 2140.
[57] J.-H. Son, M. A. Pudenz, J. D. Hoefelmeyer, *Dalton Trans.* **2010**, *39*, 11081.
[58] M. Hedidi, W. Erb, F. Lassagne, Y. S. Halauko, O. A. Ivashkevich, V. E. Matulis, T. Roisnel, G. Bentabed-Ababsa, F. Mongin, *RSC Adv.* **2016**, *6*, 63185.
[59] This is confirmed by estimating the acidity and the basicity of the B and N centres, respectively, as shown in Table S1 in the Supporting Information.
[60] É. Rochette, M.-A. Courtemanche, A. P. Pulis, W. Bi, F.-G. Fontaine, *Molecules* **2015**, *20*, 11902.

Manuscript received: February 19, 2022
Accepted manuscript online: April 21, 2022
Version of record online: May 5, 2022